Probabilities for temperature differences in Rayleigh-Bénard convection

Emily S. C. Ching
The James Franck Institute and the Department of Physics, The University of Chicago, Chicago, Illinois 60637
(Received 21 March 1991)

This paper reports the behavior of the probability density functions (PDF's) of temperature differences, between different times, but measured at the same point, which is at the center of a helium-gas cell. One objective of this work is to study how these PDF's evolve as the separation time increases. Data from seven Rayleigh numbers (Ra), which range from 10^9 to 10^{15} and are above what is called the soft-to-hard turbulence transition, are studied. These PDF's are symmetric and non-Gaussian, and are fitted approximately by a stretched-exponential form $e^{-c|x|^\beta}$. As the separation time τ increases, the parameter β starts from 0.51 ± 0.05 (for the smallest separation), remains approximately constant for $\tau \leq \tau_1$, then increases, and finally at $\tau=\tau_2$, it saturates to 1.7 ± 0.1 (1.6 ± 0.1 for the two largest Ra studied). For $\mathrm{Ra} < 7.3\times10^{10}$, β increases as $\tau^{0.27\pm0.03}$, while for $\mathrm{Ra} \geq 7.3\times10^{10}$, the increase has to be described by two powers: for lower τ, β first increases slower as $\tau^{0.15\pm0.03}$, then for $\tau \geq \tau_b$, it increases as $\tau^{0.27\pm0.02}$. Attempts are made to understand the origin of these time scales and to relate them to time scales previously identified in the problem.

Rayleigh-Bénard convection can be used for studying turbulence in fluid mechanics, which has long been a challenge to understand. By using low-temperature helium gas [1], a wide range of Rayleigh numbers can be covered. A series of experiments, directed by Libchaber [2–4] was conducted to study the transition to turbulence [2] and the properties of various statistical quantities; for example, the Nusselt number, the histogram of local temperature fluctuations, and the mean velocity field, in the different turbulent states [3,4]. These experimental studies established that there exists a transition between the soft and hard turbulence, which occurs at $\mathrm{Ra}\sim10^8$. More recently, the frequency power spectra of local temperature fluctuations in a bigger experimental cell have also been studied [5]. A change in the behavior of the power spectra was found to occur at $\mathrm{Ra}\sim10^{11}$, indicating a new regime within the hard turbulence. We have proposed the wrinkling or roughening of isothermal surfaces as a unified mechanism for all these changes or transitions [6]. In this paper, I shall present results on the probability density functions (PDF's) of temperature differences, between different times but at the same point, in the hard turbulence regime of this new cell. These PDF's and the power spectra are not unrelated. On the one hand, the structure function of temperature differences, defined as

$$S(\tau)=\langle[T(t+\tau)-T(t)]^2\rangle = 2\{\langle[T(t)]^2\rangle-\langle T(t)T(t+\tau)\rangle\}\ , \quad (1)$$

is the second moment of the PDF's. On the other hand, the frequency power spectrum is the Fourier transform of the correlation function, $\langle T(t)T(t+\tau)\rangle$. Thus, specifically, the power spectrum gives us information about how the second moments change as the separation time changes. The PDF's should therefore contain more information than the power spectra. In particular, it is interesting to understand how the PDF evolves as the separation time increases.

Previous workers [7–11] have devoted considerable efforts to the study of the small-scale structure of turbulence with a view to understanding intermittency [12]. For instance, high-order moments of the PDF (equivalent to high-order structure functions) of differences of velocity [9,10] and passive scalars, e.g., temperature [11], were measured. The intermittency parameter μ was then determined and compared with predictions by the log normal [13,14] and the β models [15]. However, it is found in this present case, the second- and higher-order structure functions do not scale with the separation time τ (except for the initial region when the separation is small enough for the difference to be approximated by the derivative).

The details of the experiment studied here have been described in previous reports [2–4]. The experimental system is a cylindrical cell, of 20 cm diameter and 40 cm height, filled with helium gas at about 5 K. The cell is heated from below by a dc power input and the temperature of the top plate is regulated. Local temperature fluctuations at various points inside the cell are measured by arsenic-doped silicon bolometers of about 0.2 mm in size. The control parameter in this experiment is the Rayleigh number which is defined as

$$\mathrm{Ra}=\frac{\alpha g \Delta L^3}{\nu\kappa}\ , \quad (2)$$

where α is the volume expansion coefficient, g is the acceleration due to gravity, Δ is the measured temperature difference between the bottom and top of the cell, L is the height of the cell, and ν and κ are, respectively, the kinematic viscosity and the thermal diffusivity of the helium gas. Using κ and L, we can construct a diffusive time scale L^2/κ [which is similar to the viscous time scale L^2/ν, as the Prandtl number ($=\nu/\kappa$) is of order 1 in this

experiment]. For the rest of the paper, we shall use this time scale, L^2/κ, and its inverse to normalize times and frequencies, respectively.

I shall concentrate on results at the center of the cell, as the flow there is believed to be characteristic of free convection flow. Results of one Rayleigh number are used for illustration and the differences for the other Rayleigh numbers are pointed out when necessary. The Rayleigh number taken is 7.3×10^{10}. A typical time recording of temperature fluctuations is shown in Fig. 1(a). The data are normalized by the root-mean-square fluctuations, denoted by Δ_c. The PDF of these normalized fluctuations is shown in Fig. 1(b). [The PDF is not as exponential as found before in the smaller (aspect-ratio one) cell [2,4] but it is clearly non-Gaussian.] We define T_τ to be the temperature difference over a time interval τ that is 2^n times the experimental sampling interval τ_0,

$$T_\tau = T(t+\tau) - T(t) \quad \text{where } \tau = 2^n \tau_0 \, . \tag{3}$$

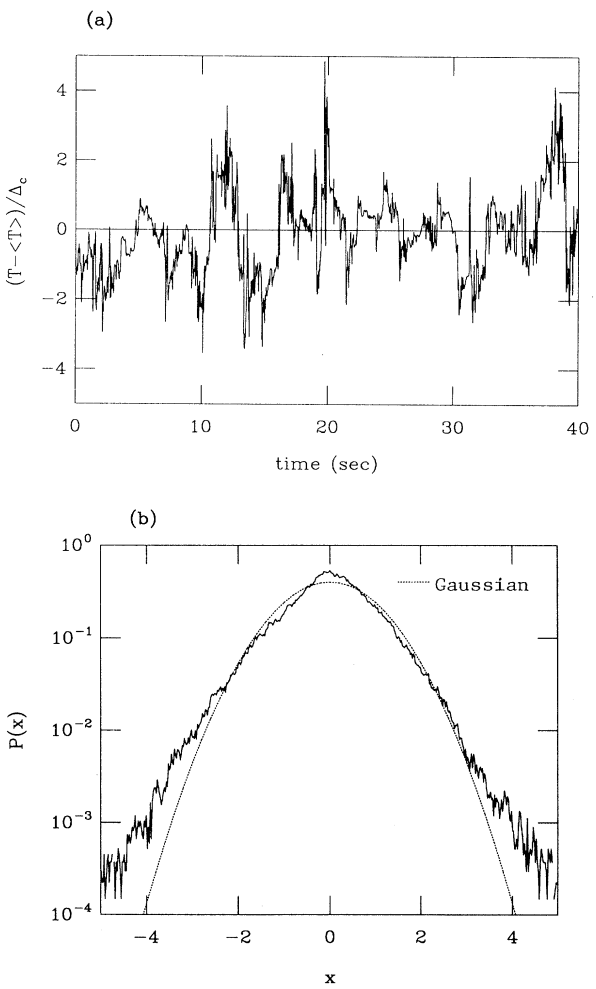

FIG. 1. A typical time recording of the temperature fluctuations normalized by the root-mean-squared fluctuations Δ_c and the corresponding PDF, $P(x)$ with $x=(T-\langle T\rangle)/\Delta_c$, at the center of the cell for $\mathrm{Ra}=7.3\times10^{10}$. The dotted line is the standard Gaussian distribution.

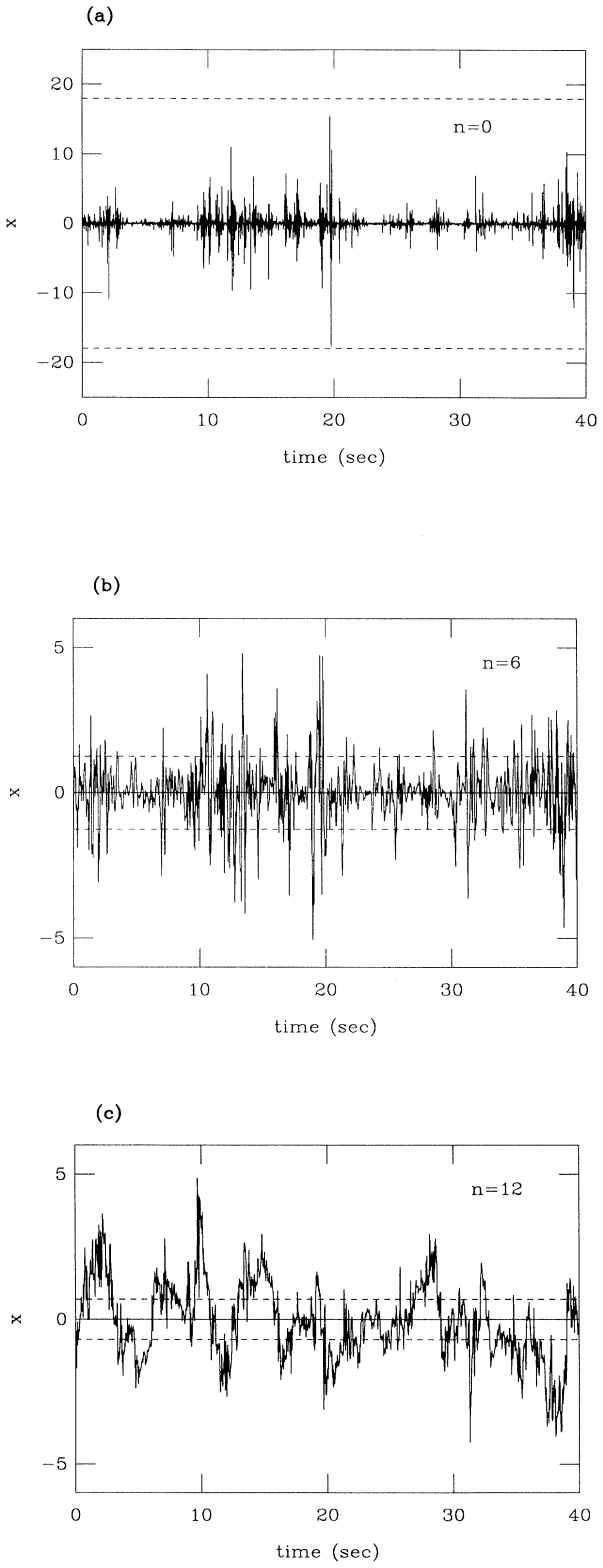

FIG. 2. Time recordings of the various T_τ [see Eq. (3)] normalized by $(\langle T_\tau^2\rangle)^{1/2}$ at the same Rayleigh number 7.3×10^{10}. x is $T_\tau/(\langle T_\tau^2\rangle)^{1/2}$ with $\tau=2^n\tau_0$, where τ_0 is the experimental sampling intervals. (a) $n=0$, (b) $n=6$, and (c) $n=12$. The dashed lines are the position of $\pm\Delta_c$.

The time recordings of T_τ, normalized by their root mean squares $(\langle T_\tau^2 \rangle)^{1/2}$, with $n=0$, 6, and 12, are shown in Figs. 2(a), 2(b), and 2(c), respectively. For comparison, Δ_c is also shown in these figures (the dotted line). For $n=0$, it is more probable to have large temperature differences relative to the root mean square (but smaller than Δ_c) and the data look quite different from the original temperature fluctuations. As n increases, the temperature differences resemble more the original temperature fluctuations shown in Fig. 1(a).

The PDF's of these temperature differences are computed from the corresponding histograms (the number of bins used ranges from 650 to 1000) and are shown in Fig. 3. It has been checked that the PDF for $n=12$ is like that for very large n. In fact, for large enough τ, $T(t+\tau)$ becomes statistically independent of $T(t)$, so we have

$$f(T_\tau)=\tfrac{1}{2}\int_{-\infty}^{\infty}[P(T)P(T+T_\tau)+P(T-T_\tau)P(T)]dT\ , \tag{4}$$

where $f(T_\tau)$ is the PDF of temperature difference separated by time τ; $P(T)$ is the PDF of the original temperature fluctuations. One sees that $f(T_\tau)$ is always symmetric for large enough τ. Another way to check that the PDF for $n=12$ is already asymptotic is to look at the root mean square of the temperature differences, $\Delta T_{\rm rms}(\tau)$, which is the square root of the second moments:

$$\Delta T_{\rm rms}(\tau)=\{\langle[T(t+\tau)-T(t)]^2\rangle\}^{1/2} = \left[\int_{-\infty}^{\infty}T_\tau^2 f(T_\tau)dT_\tau\right]^{1/2}. \tag{5}$$

Thus $\Delta T_{\rm rms}(\tau)$ is the square root of the structure function, which is related to the frequency power spectra, as mentioned before. The log-log plot of $\Delta T_{\rm rms}(\tau)$ as a function of τ is presented in Fig. 4. As τ increases, $T(t+\tau)$ and $T(t)$ decorrelate, with the correlation function $\langle T(t)T(t+\tau)\rangle$ becoming $\langle T\rangle^2$, and $\Delta T_{\rm rms}(\tau)$ tending to $\sqrt{2}\Delta_c$ [see Eq. (1)]. The decorrelation time $\tau_{\rm dec}$ can be estimated from the beginning of the flat region in the curve. We expect $T(t+\tau)$ and $T(t)$ to become statistically independent of each other when τ is of the order of $\tau_{\rm dec}$ and we check that $n=12$ lies in the flat region of the curve in Fig. 4.

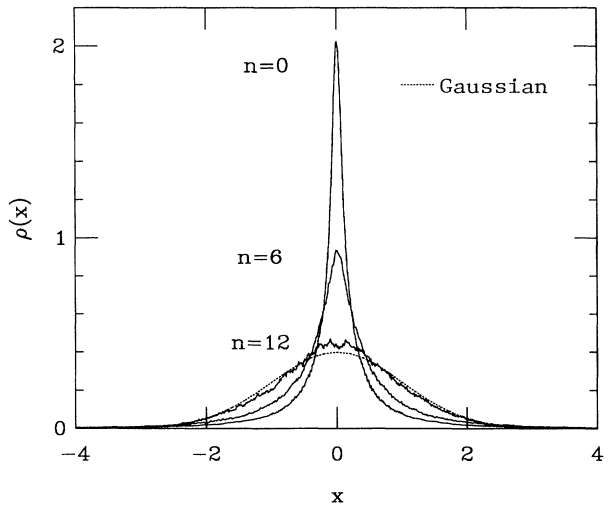

FIG. 3. Probability density functions (PDF's) of the normalized temperature differences for the three cases in Fig. 2. Again x is $T_\tau/(\langle T_\tau^2\rangle)^{1/2}$ with $\tau=2^n\tau_0$ as defined in Eq. (3). The dotted line is the standard Gaussian distribution.

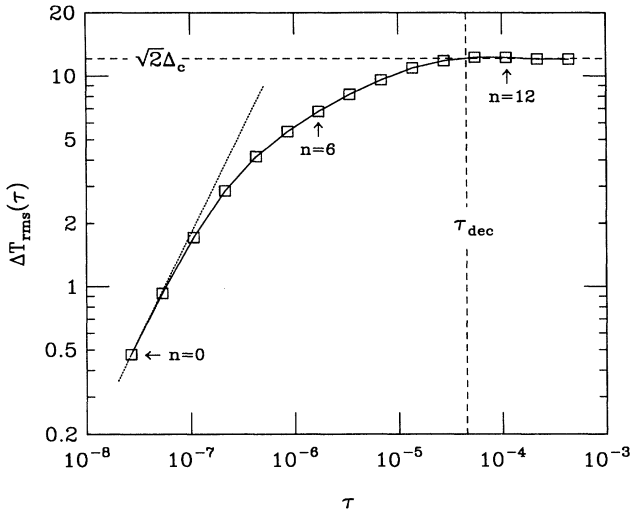

FIG. 4. Root mean square of the temperature differences $\Delta T_{\rm rms}(\tau)$, as a function of τ for $\mathrm{Ra}=7.3\times10^{10}$. τ is in units of L^2/κ. For small τ, $\Delta T_{\rm rms}(\tau)$ increases linearly in τ. The dotted line is a line of slope one in the log-log plot. The time for $T(t+\tau)$ and $T(t)$ to decorrelate, $\tau_{\rm dec}$, is also shown.

Returning to Fig. 3, we notice that the PDF's are essentially symmetric. For comparison purposes, the PDF's are normalized such that the second moment is equal to 1:

$$\int_{-\infty}^{\infty}x^2\rho(x)dx=1\ , \tag{6}$$

where $x=T_\tau/(\langle T_\tau^2\rangle)^{1/2}$ [$\rho(x)=f(T_\tau)(\langle T_\tau^2\rangle)^{1/2}$]. Note also that these PDF's have a non-Gaussian shape. The peak value is larger than that of the Gaussian distribution, but the difference decreases as τ increases.

The non-Gaussian shape of PDF's is not unfamiliar. In fact, $P(T)$ itself is non-Gaussian [2,4] [see Fig. 1(b)]. This has stimulated some recent theoretical works [16–22]. Measurements made by Gagne [23] on velocity and temperature differences in high-Reynolds-number turbulence also revealed similar shapes to the ones observed here. To explain the statistics of these velocity differences, Castaing, Gagne, and Hopfinger [24] have developed a model based on the superposition of approximately Gaussian PDF's whose invariances have log normal distributions. Several recent numerical simulations of both shear turbulence [25–27] and convective turbulence [28,29] have also found non-Gaussian PDF's of velocity and temperature gradients.

One objective of this work is to study how the PDF

evolves as τ increases. To this end, we fit the PDF by a stretched-exponential form [29]

$$\rho(x)=\rho(0)e^{-c|x|^{\beta}}, \quad c,\beta>0 \ . \tag{7}$$

Note that $\beta=2$ corresponds to Gaussian distribution and $\beta=1$ corresponds to exponential distribution, while $\beta<1$ indicates a flatter intermittent distribution. We also note that the stretched-exponential form appears to be a very general form for relaxation phenomena in condensed-matter physics [30,31].

In order to obtain estimates for the parameters c and β, $\rho(0)$ is taken from the data and $\ln\{\ln[\rho(0)/\rho(x)]\}$ is plotted versus $\ln|x|$. If Eq. (7) is a good representation of the PDF, a straight line with slope β and y intercept $\ln c$ will be obtained. If the PDF's are symmetric, plots for $x>0$ and $x<0$ should give the same results. It is found that a reasonably good straight line is obtained for a region near the tail of the PDF. A least-squares fit to this region gives estimates for the slope and y intercept. The values of c and β are obtained by taking the average of these estimates from both the $x>0$ and $x<0$ curves. Note that the fitted form obtained this way may not have the correct normalization, $\int_{-\infty}^{\infty}\rho(x)dx=1$. With these values of c and β, the PDF's are compared with Eq. (7). The comparisons are shown in Fig. 5. We see that, except around the peak region, Eq. (7) fits well for the PDF's in all the three cases. This is different from the hyperbolic intermittency $[\rho(x)\sim x^{-\alpha}$ for large $x]$ ob-

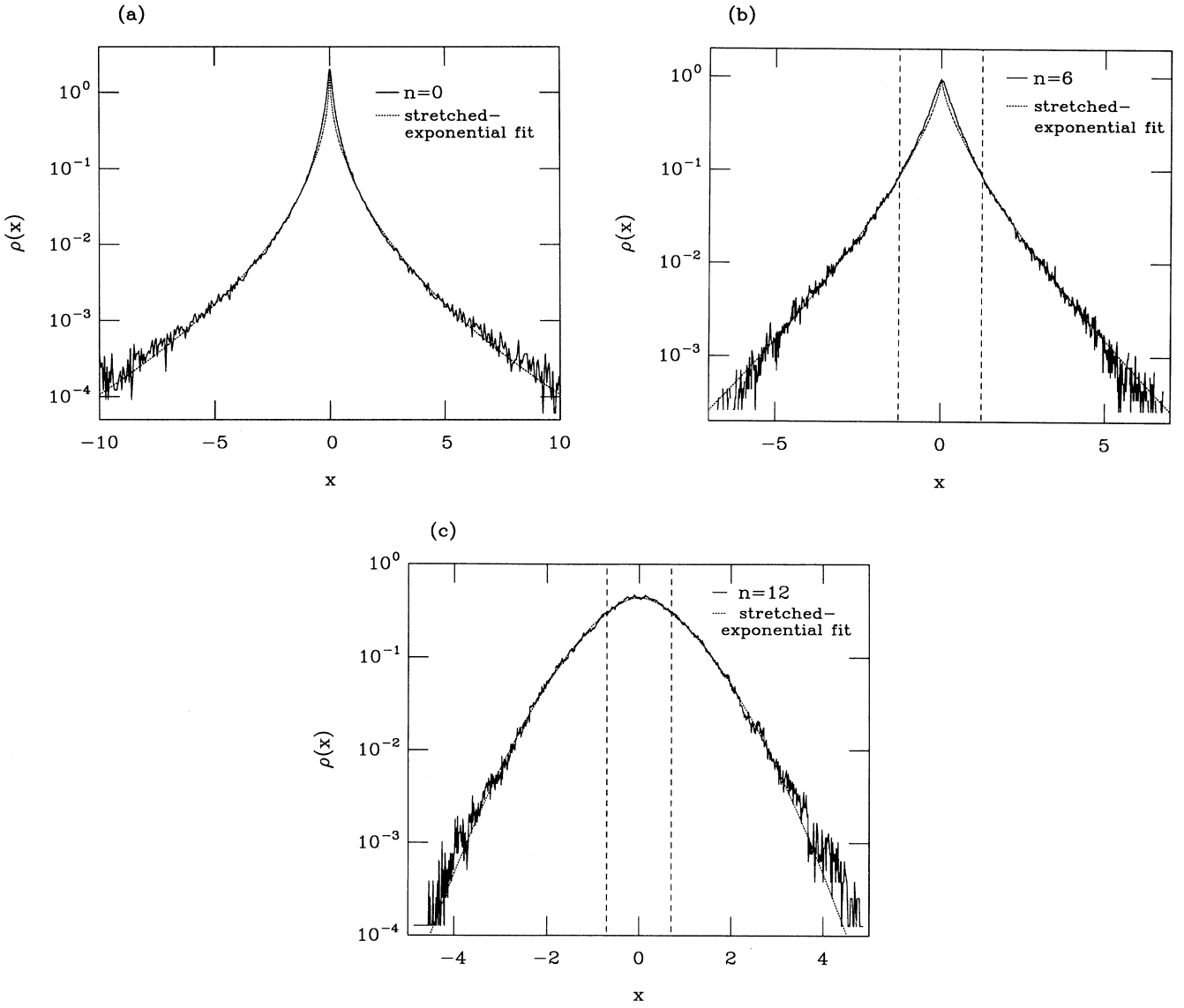

FIG. 5. Comparison of the stretched-exponential forms [Eq. (7)] with the PDF's for $\mathrm{Ra}=7.3\times10^{10}$. The dotted line is the fitted form and the solid line is the PDF $\rho(x)$ and $x=T_\tau/(\langle T_\tau^2\rangle)^{1/2}$ and $\tau=2^n\tau_0$. (a) $n=0$, (b) $n=6$, and (c) $n=12$. The positions of $\pm\Delta_c$ are shown as dashed lines.

tained by Schertzer and Lovejoy [32] in atmospheric dynamics. For $n=0$ and 6, the peaks of the PDF's are more rounded off than the fitted form. The β values obtained in these cases are less than 1 (see Fig. 6), so that the fitted forms have infinite slopes when approaching from both sides of the peak. Since the PDF is smooth, we expect the fit not to work near the peak region.

The evolution of β as a function of τ is plotted in Fig. 6. When plotted in a log-log graph, the $\beta(\tau)$ curve can reasonably be fitted by four straight lines as shown. That is, β starts at 0.47 ± 0.01, remains approximately constant for $\tau\leq\tau_1$, then it increases as $\tau^{0.17\pm0.02}$. At $\tau\sim\tau_b$, the rate of increase is faster and β increases as $\tau^{0.27\pm0.02}$. Finally, at $\tau=\tau_2$, it saturates at a value of 1.7 ± 0.1. This behavior of β is basically the same for $\mathrm{Ra}\geq7.3\times10^{10}$, with the average values of the first and second powers equal to 0.15 ± 0.03 and 0.27 ± 0.02, respectively. However, for $\mathrm{Ra}=6.0\times10^{8}$ and 4.0×10^{9}, the rate of increase is described by a single power, $\sim\tau^{0.27\pm0.03}$, so the time scale τ_b is not present. The average initial value of β is 0.51 ± 0.05. This is consistent with what Gagne [23] found for PDF's of velocity and temperature differences for separation lying in the dissipative range. The average saturated value is 1.7 ± 0.1 for the five smaller Rayleigh numbers (with $\mathrm{Ra}<10^{13}$) and 1.6 ± 0.1 for the two largest Ra. The $\beta(\tau)$ curves for the seven Rayleigh numbers studied are plotted in Fig. 7.

In the following, we shall try to understand the shape of the $\beta(\tau)$ curves and the origin of the different time scales. The saturation region at large τ is easily understood:

$$\rho(x)\equiv\rho\left[\frac{T_\tau}{[\langle(T_\tau)^2\rangle]^{1/2}}\right]=f(T_\tau)[\langle(T_\tau)^2\rangle]^{1/2}\ . \tag{8}$$

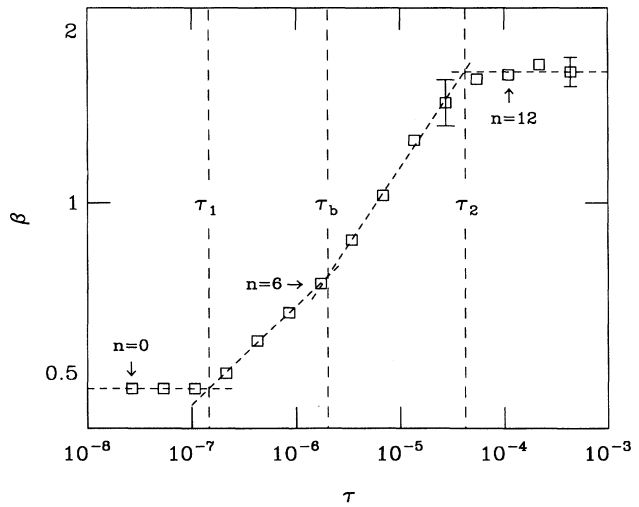

FIG. 6. Dependence of the parameter β in the stretched-exponential fit [see Eq. (7)] as a function of the separation time $\tau=2^n\tau_0$ for $\mathrm{Ra}=7.3\times10^{10}$. The three time scales τ_1, τ_b, and τ_2 are indicated. The times are normalized by L^2/κ. The biggest errors in β are also shown.

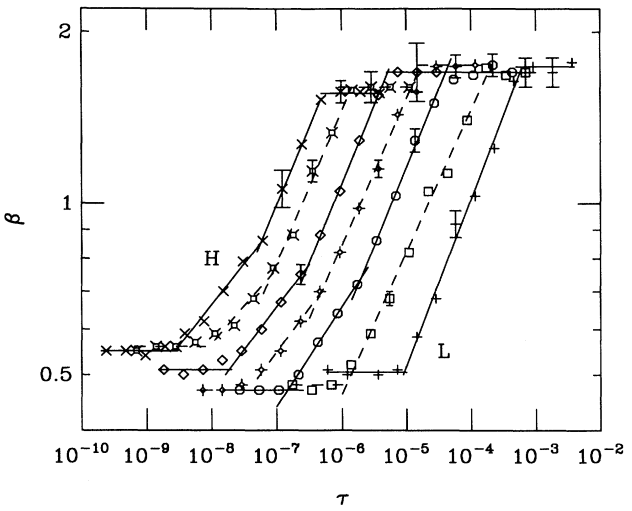

FIG. 7. The $\beta(\tau)$ curves for $\mathrm{Ra}=6.0\times10^{8}$, 4.0×10^{9}, 7.3×10^{10}, 6.0×10^{11}, 6.7×10^{12}, 4.1×10^{13}, and 5.8×10^{14}. The curves L and H are for the lowest and highest Ra, respectively. τ is in units of L^2/κ. The biggest errors in β are also shown.

As mentioned before, both $f(T_\tau)$ and $[\langle(T_\tau)^2\rangle]^{1/2}$ $[=\sqrt{S(\tau)}]$ become independent of τ, and so are $\rho(x)$ and β, when τ is larger than τ_{dec}. Thus we have $\tau_2\sim\tau_{\mathrm{dec}}$. We expect the decorrelation time to be of the order of the turnover time of the large-scale flow. This turnover time was estimated previously [2,5] as $1/\omega_p$ where ω_p is the outer frequency scale in the power spectra of the temperature fluctuations [5], which was found to scale as $\mathrm{Ra}^{1/2}$. For this new experimental cell, we confirmed this $\mathrm{Ra}^{1/2}$ dependence, and the prefactor is found to be 0.08, namely,

$$\omega_p=0.08\mathrm{Ra}^{0.5}\ . \tag{9}$$

In Fig. 8, we compare τ_2, τ_{dec}, and $1/\omega_p$. The agreement is good; thus we can conclude that τ_{dec} and τ_2 essentially describe the same physics as ω_p.

To understand the flat region for small τ, recall that

$$x=\frac{T(t+\tau)-T(t)}{\{\langle[T(t+\tau)-T(t)]^2\rangle\}^{1/2}}\ .$$

If we assume that $T(t)$ is differentiable, we get

$$\rho(x)=\rho\left[\frac{T'(t)}{\{\langle[T'(t)]^2\rangle\}^{1/2}}\right][1+O(\tau)]\ . \tag{10}$$

Thus for small enough τ, $\rho(x)$ is approximately independent of τ again. One way to estimate this small τ is to check when the approximation

$$T(t+\tau)-T(t)\sim\tau T'(t) \tag{11}$$

fails. Recall from Eq. (5),

$$\Delta T_{\mathrm{rms}}(\tau)=\tau\{\langle[T'(t)]^2\rangle\}^{1/2}\left[1-\frac{\tau^2}{24}\frac{\langle[T''(t)]^2\rangle}{\langle[T'(t)]^2\rangle}+O(\tau^3)\right]\ . \tag{12}$$

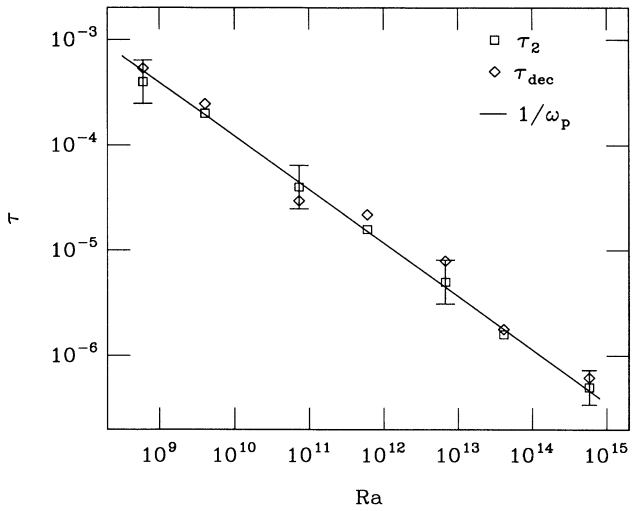

FIG. 8. Comparison of the three time scales τ_2, τ_{dec}, and $1/\omega_p$. The time scale τ_2 is obtained from the saturation region of the β curves in Fig. 7, while τ_{dec} is the decorrelation time estimated from the flat region in the $\Delta T_{rms}(\tau)$ curves (see Fig. 4) and $1/\omega_p$ (solid line) is the estimated turnover time of the large-scale flow. All the time scales are normalized by L^2/κ. Errors for every second data point of τ_2 are shown.

If Eq. (11) holds, $\Delta T_{rms}(\tau)$ should increase linearly in τ for small τ. This is confirmed by the data presented in Fig. 4. We define τ_s to be the time when the piecewise slope of $\Delta T_{rms}(\tau)$ in the log-log plot equals 0.9. From Eq. (12), we find

$$\tau_s \sim \left[\frac{6}{5} \frac{\langle [T'(\tau)]^2 \rangle}{\langle [T''(t)]^2 \rangle} \right]^{1/2} . \tag{13}$$

[This definition of τ_s is quite arbitrary and we expect that the correction terms in Eqs. (10) and (12) are in general different, so our purpose is to see whether τ_s and τ_1 are of the same order of magnitude.] We note also that the averages of the temperature derivatives are just integrals involving the frequency power spectrum. Thus we can also write

$$\tau_s \sim \frac{1}{2\pi} \left[\frac{6}{5} \frac{\int \omega^2 P(\omega) d\omega}{\int \omega^4 P(\omega) d\omega} \right]^{1/2} , \tag{14}$$

where $P(\omega)$ is the frequency power spectrum. [$P(\omega)$ equals to $|\int_0^t T(t') e^{i2\pi\omega t'} dt'|^2/t$, i.e., ω is just the frequency but not angular frequency.] It was found [5] that for $\mathrm{Ra} \lesssim 10^{11}$, the power spectrum $P(\omega)$ is well approximated by a power law followed by an exponential decay, namely,

$$P(\omega) \sim \left[\frac{\omega}{\omega_p} \right]^{-7/5} e^{-\omega/\omega_d} \quad \text{for } \omega > \omega_p . \tag{15}$$

This conforms to the standard thinking about power spectra in turbulence [33]. The frequency ω_d is the frequency above which dissipation becomes important and is the analog of the Kolmogorov length scale. Thus, for $\mathrm{Ra} \lesssim 10^{11}$, one gets

$$\tau_s \sim \tau_d \equiv \frac{5}{4\pi} \left[\frac{3}{65} \right]^{1/2} \frac{1}{\omega_d} . \tag{16}$$

For $\mathrm{Ra} > 10^{11}$, Eq. (15) no longer holds and the functional form of $P(\omega)$ is not known *a priori*. Thus, there is not a corresponding well-defined dissipative frequency or time scale in this regime. We plot τ_s [computed using Eq. (13)], τ_d (with ω_d obtained from Ref. [6]), and τ_1 in Fig. 9. As expected, τ_d agrees with τ_s for $\mathrm{Ra} \lesssim 10^{11}$. Both of them are about the same order of magnitude as τ_1 and have the same Rayleigh-number dependence for $\mathrm{Ra} < 10^{12}$. Thus for $\mathrm{Ra} < 10^{12}$, τ_1 is just $1/\omega_d$ up to a prefactor of order 0.1. However, for $\mathrm{Ra} \gtrsim 10^{12}$, τ_s deviates from τ_1 significantly; in particular, the two time scales have a different dependence on Ra. This change occurs at about the same Rayleigh number at which the power spectrum of temperature fluctuations changes behavior [5]. In Ref. [6], we suggested that the change in power spectra is a result of the roughening of the thermal plumes. Another interesting thing to note is that τ_1 scales as a power of Ra:

$$\tau_1 \sim \mathrm{Ra}^{-x} , \tag{17}$$

with $x = 0.73 \pm 0.06$ and 0.4 ± 0.1 below and above $\mathrm{Ra} \sim 10^{11}$, respectively. The first exponent agrees with the result [6] that

$$\omega_d \sim \mathrm{Ra}^{0.79 \pm 0.06} \quad \text{for } \mathrm{Ra} \lesssim 10^{11} . \tag{18}$$

The second exponent, 0.4 ± 0.1, is consistent with the exponent obtained for $\{\langle [T'(t)]^2 \rangle\}^{1/2}$. In Ref. [6], we

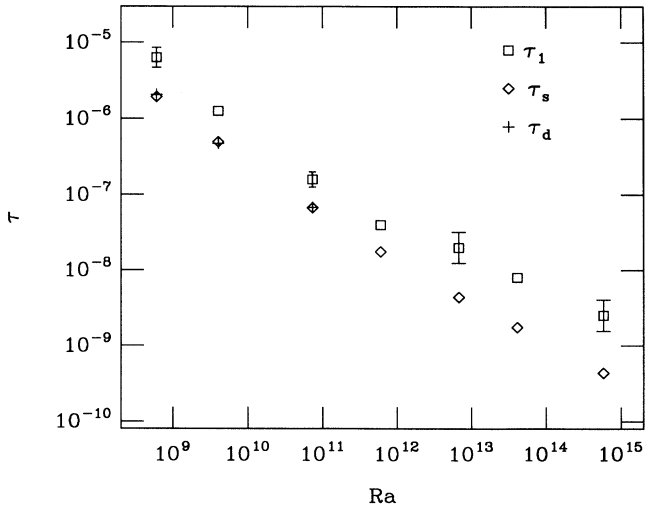

FIG. 9. Comparison of the time scales τ_1, τ_s, and τ_d. The time scale τ_1 is obtained from the initial flat region of the β curves, while τ_s is computed using Eq. (13) and τ_d is $1/\omega_d$ up to a prefactor of order 0.1 [see Eq. (16)]. All the time scales are normalized by L^2/κ. Errors for every second data point of τ_1 are shown.

found that

$$Q \equiv \frac{\{\langle [T'(t)]^2 \rangle\}^{1/2}}{\Delta_c \kappa / L^2} \sim \mathrm{Ra}^y , \tag{19}$$

with $y = 0.48 \pm 0.06$ for Ra above $\sim 10^{11}$.

One last thing is to understand the time scale τ_b. As mentioned before in Eq. (15), the power spectra can be approximated by a power law followed by an exponential decay for $\mathrm{Ra} \lesssim 10^{11}$. For $\mathrm{Ra} \gtrsim 10^{11}$, Eq. (15) no longer holds [5] but nevertheless there is still a power-law region of exponent $-\frac{7}{5}$. We define ω_b to be the highest frequency when this power law ends. [Strictly speaking, this is not too well defined for $\mathrm{Ra} \gtrsim 10^{11}$, as the functional form of $P(\omega)$ is not known. However, one can still get a rough estimate of this frequency.] This frequency ω_b is measured from the power spectra obtained in Ref. [5]. The comparison of τ_b and $1/\omega_b$ is shown in Fig. 10. The agreement is not too good but the two time scales are about the same order. If we fit the scattered data points of τ_b by a power law, we find

$$\tau_b \sim \mathrm{Ra}^{-(0.4 \pm 0.1)} , \tag{20}$$

which again has an exponent similar to τ_1 and Q^{-1} for $\mathrm{Ra} \gtrsim 10^{11}$.

To conclude, the PDF's of temperature differences are fitted by a stretched-exponential form $e^{-c|x|^\beta}$. The behavior of these PDF's as a function of the separation time is then studied through the β curves. From the shape of the β curves, one can identify three time scales, τ_1, τ_b, and τ_2 (τ_b is not relevant for $\mathrm{Ra} < 7.3 \times 10^{10}$). One finds that τ_2 is just $1/\omega_p$ and describes the decorrelation time or the turnover time. For $\mathrm{Ra} \lesssim 10^{11}$, τ_1 is $1/\omega_d$ up to a small prefactor of order 0.1. For $\mathrm{Ra} \gtrsim 10^{11}$, τ_1 and τ_b (and also Q^{-1}) have a similar Rayleigh number dependence, $\sim \mathrm{Ra}^{-(0.4 \pm 0.1)}$. The time scale τ_b is found to be related to the frequency ω_b at which the $-\frac{7}{5}$ power law ends. For $\mathrm{Ra} \lesssim 10^{11}$, ω_b is just ω_d up to a prefactor, but for $\mathrm{Ra} \gtrsim 10^{11}$, ω_b behaves differently. Thus a time scale scaling as $\mathrm{Ra}^{-(0.4 \pm 0.1)}$ appears, which may be associated with the roughening transition of the thermal plumes [6], but its precise physical meaning has still to be understood.

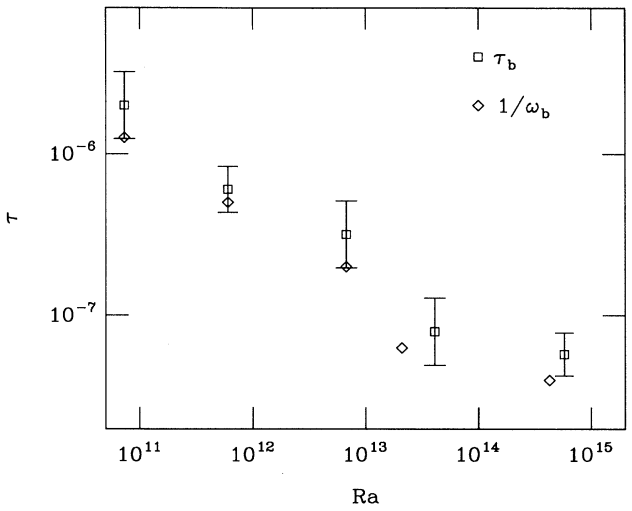

FIG. 10. Comparison of τ_b with $1/\omega_b$. The time scale τ_b is defined only for $\mathrm{Ra} \geq 7.3 \times 10^{10}$ (see Fig. 6 for illustration). The frequency ω_b is defined as the higher end of the $-\frac{7}{5}$ power law in the power spectra of temperature fluctuations. All the time scales are normalized by L^2/κ. The errors in $1/\omega_b$ are similar to those shown for τ_b.

I thank L. Kadanoff for his guidance in this work and his critical reading of the manuscript. I have also benefited from many discussions with A. Libchaber, I. Procaccia, X. Z. Wu, and R. Zeitak. Finally, I am grateful to G. Yates of the Social Sciences and Public Policy Computing Center in University of Chicago for his help in the data transfer. This work is supported by NSF Grant No. DMR 8815895.

[1] D. C. Threlfall, Ph.D. thesis, University of Cambridge, 1976 (unpublished); J. Fluid Mech. **67**, 17 (1975).
[2] F. Heslot, B. Castaing, and A. Libchaber, Phys. Rev. A **36**, 5870 (1987).
[3] B. Castaing, G. Gunaratne, F. Heslot, L. Kadanoff, A. Libchaber, S. Thomae, X. Z. Wu, S. Zaleski, and G. Zanetti, J. Fluid Mech. **204**, 1 (1989).
[4] M. Sano, X. Z. Wu, and A. Libchaber, Phys. Rev. A **40**, 6421 (1989).
[5] X. Z. Wu, L. Kadanoff, A. Libchaber, and M. Sano, Phys. Rev. Lett. **64**, 2140 (1990).
[6] I. Procaccia, E. S. C. Ching, P. Constantin, L. P. Kadanoff, A. Libchaber, and X. Z. Wu (unpublished).
[7] K. R. Sreenivasan and R. A. Antonia, Phys. Fluids **20**, 1238 (1977).
[8] C. Meneveau and K. R. Sreenivasan, Nucl. Phys. (Proc. Suppl.) B **2**, 49 (1987).
[9] R. A. Antonia, B. R. Satyaprakash, and A. J. Chambers, Phys. Fluids **25**, 29 (1982).
[10] F. S. Anselmet, Y. Gagne, E. J. Hopfinger, and R. A. Antonia, J. Fluid Mech. **140**, 63 (1984).
[11] R. A. Antonia, E. J. Hopfinger, Y. Gagne, and F. Anselmet, Phys. Rev. A **30**, 2704 (1984).
[12] For a discussion, see A. S. Monin and A. M. Yaglom, *Statistical Fluid Mechanics Vol. 2* (MIT Press, Cambridge, MA, 1975).
[13] A. N. Kolmogorov, J. Fluid Mech. **13**, 82 (1962).
[14] A. M. Obukhov, J. Fluid Mech. **13**, 77 (1962).
[15] U. Frisch, P.-L. Sulem, and M. Nelkin, J. Fluid Mech. **87**, 719 (1978).
[16] Y. G. Sinai and V. Yakhot, Phys. Rev. Lett. **63**, 1962 (1989).
[17] V. Yakhot, Phys. Rev. Lett. **63**, 1965 (1989).
[18] H. Chen, S. Chen, and R. H. Kraichnan, Phys. Rev. Lett.

63, 2657 (1989).
[19] R. H. Kraichnan, Phys. Rev. Lett. **65**, 575 (1990).
[20] Z.-S. She, Phys. Rev. Lett. **66**, 600 (1991).
[21] Z.-S. She and S. A. Orszag, Phys. Rev. Lett. **66**, 1701 (1991).
[22] A. Pumir, B. I. Shraiman, and E. D. Siggia, Phys. Rev. Lett. **66**, 2984 (1991).
[23] Y. Gagne, Ph.D. thesis, Institut National Polytechnique de Grenoble (unpublished).
[24] B. Castaing, Y. Gagne, and E. J. Hopfinger, Physica D **46**, 177 (1990).
[25] K. Yamamoto and I. Hosokawa, J. Phys. Soc. Jpn. **57**, 1532 (1988).
[26] I. Hosokawa and K. Yamamoto, J. Phys. Soc. Jpn. **58**, 20 (1989).
[27] S. Kida and Y. Murakami, Fluid Dyn. Res. **4**, 347 (1989).
[28] E. E. DeLuca, J. Werne, R. Rosner, and F. Cattaneo, Phys. Rev. Lett. **64**, 2370 (1990).
[29] S. Balachandar and L. Sirvoich, Phys. Fluids A **3**, 919 (1991).
[30] V. Degiorgio, T. Bellini, R. Piazza, F. Mantegazza, and R. E. Goldstein, Phys. Rev. Lett. **64**, 1043 (1990).
[31] K. L. Ngai, Comments Solid State Phys. **9**, 127 (1979).
[32] D. Schertzer and S. Lovejoy, Turbulent Shear Flow **4**, 7 (1985).
[33] A. N. Kolmogorov, C. R. Acad. Sci. U.S.S.R. **30**, 301 (1941); **30**, 538 (1941).